Title

Characterization of scatterer motion in a reverberant medium

Journal

Journal of the Acoustical Society of America, 119(2)

ISSN

0001-4966

Authors

Conti, Stephane G

de Rosny, J

Roux, P

et al.

Publication Date

2006-02-01

Peer reviewed

Characterization of scatterer motion in a reverberant medium

Stéphane G. Conti[a)]
Southwest Fisheries Science Center, 8604 La Jolla Shores Drive, La Jolla, California, 92037

Julien de Rosny
Laboratoire Ondes et Acoustique, 10 Rue Vauquelin, 75005, Paris, France

Philippe Roux
Marine Physical Laboratory, SIO/UCSD, 9500 Gilman Dr., La Jolla, California 92093-0205

David A. Demer
Southwest Fisheries Science Center, 8604 La Jolla Shores Drive, La Jolla, California, 92037

(Received 20 April 2005; revised 9 November 2005; accepted 9 November 2005)

Recently, an acoustic technique has been proposed to measure the scattering strength and the dynamics of weak moving scatterers in a reverberant cavity: diffusing reverberant acoustic wave spectroscopy (DRAWS). Both parameters are obtained from the correlations of the reverberated-scattered transient pressure fields for different scatterers positions. This technique is based on a diffusive field theory [de Rosny *et al.*, Phys. Rev. Lett., **90**, 094302 (2003)]. Here, a more systematic approach of the DRAWS technique properties is presented. Moreover, an important extension is proposed using the fourth-order moment of the field, or the variance of the correlation estimator. Contrary to the correlations (second-order moment) that allow the measurement of the scattering cross section, its variance (fourth-order moment) is shown to be mainly sensitive to the scatterer displacement. The robustness of DRAWS is discussed using different configurations: a computer simulation of a moving scatterer in a two-dimensional cavity. Experiments were also carried out with a 23-mm-diameter copper sphere moved by stepping motors in 16 liters of water, and finally a human walking in a 125-m^3 reverberant room. © *2006 Acoustical Society of America.* [DOI: 10.1121/1.2146107]

PACS number(s): 43.20.El, 43.20.Ye, 43.30.Gv, 43.80.Ev [EJS] Pages: 769–776

I. INTRODUCTION

In the last decades, techniques based on multiply scattered waves have been developed to characterize clouds of moving scatterers. Conventional techniques such as Doppler imaging cannot be applied in this case because they are based on a single scattering approximation. To overcome this limitation, the diffusing wave spectroscopy (DWS; Maret and Wolf, 1987; Pine *et al.*, 1988) has been developed in optics to measure the diffusion constant of Brownian scatterers from the temporal fluctuations of the speckle of a multiply scattered laser beam. Later, DWS was extended to acoustic waves with the diffusing acoustic wave spectroscopy (DAWS; Cowan *et al.*, 2000; 2002). In acoustics, one can easily record the transient acoustic response of the multiple scattering medium. Therefore, more information can be obtained from the field fluctuations with respect to the propagation length, i.e., the scattering order. Finally, for weak scatterers in motion in a strongly reverberant medium, it has been recently demonstrated that the acoustical total scattering cross section σ_T can be determined from an ensemble of transient pressure fields recorded for uncorrelated positions of the scatterer (de Rosny, 2000; de Rosny and Roux, 2001). It was shown that the ratio of the coherent intensity (square of the sum of the transient responses) and the incoherent intensity (sum of the squared transient responses) decreases as $\exp(-L/l_s)$, where L is the acoustic path, and l_s the mean free path. Later, a more general approach was developed in the case of a single scatterer (de Rosny *et al.*, 2003). Like DWS, it consists of studying the normalized correlations between transient fields recorded at a given propagation time for two different positions of one scatterer. These works led to the diffusing reverberant acoustic wave spectroscopy (DRAWS), where the dynamics and the total scattering cross section σ_T can be estimated from normalized field correlations. DRAWS is based on two main assumptions. First, the mean free path l_s of the scatterer is much larger than the dimensions of the cavity. Second, the wave is reflected multiple times on the boundary of the cavity before extinction. The last assumption implies that the field is diffuse in the sense of room acoustics theory (Schroeder, 1959), i.e., it is isotropic and homogeneous.

The accuracy and precision of DRAWS to measure the total scattering cross section σ_T was characterized using standard metal spheres in water for ultrasonic waves (Demer *et al.*, 2003). DRAWS was since used successfully to measure σ_T for Antarctic and Northern krill in small seawater containers with ultrasonic waves (Demer and Conti, 2003; Conti *et al.*, 2005), for fish in large seawater tanks with ultrasonic waves (Conti and Demer, 2003), and for humans in air with audible acoustic waves (Conti *et al.*, 2004).

[a)]Author to whom correspondence should be addressed. Electronic mail: sconti@ucsd.edu

However, the ability of DRAWS to characterize the average scatterer motion was investigated only once by de Rosny *et al.* (2003). Here, we propose a more detailed investigation of DRAWS to characterize the type and magnitude of the scatterer displacement. Also, we extend the DRAWS theory and demonstrate that the variance of the correlated field for two positions of a scatterer can provide a metric for the magnitude of the scatterer displacement, independently of the total scattering cross section.

The theoretical principles are confirmed first using simulations for a single scatterer in a two-dimensional reverberant cavity, and then experimentally with a standard metal sphere in a stainless-steel bucket filled with water for ultrasonic waves, and with a human in a squash court for the audible range.

II. FORMALISM

A. Theory

Consider a reverberant cavity of volume V with one fixed transducer transmitting N pulses at a constant repetition rate. For each pulse, transient fields in the cavity are recorded by one or more receivers. One scatterer is moving by constant steps δx in the cavity between each of the N pulses. The average displacement of the scatterer after n steps is denoted as $\delta r(n)$. For the pulse k, the transient field is denoted as $h_k(t)$, with k ranging from 1 to N. After n steps, the coherent intensity (the cross correlation) and the incoherent intensity (the autocorrelation) of the $h_k(t)$ are, respectively, $I_n(t) = \langle h_k(t) h_{k+n}(t) \rangle$ and $A(t) = \langle h_k(t)^2 \rangle$, where $\langle \cdot \rangle$ is the average over the N pulses (Ishimaru, 1978; Sheng, 1995).

When the positions of the scatterer are uncorrelated between transient fields, de Rosny and Roux (2001) demonstrated that the normalized cross-correlation function $g_1^t(n=1) = [I_1(t)]/[A(t)]$ of $h_k(t)$ and $h_{k+1}(t)$, decreases exponentially with the scattering mean free path l_s: $g_1^t(n=1) \approx \exp(-tc/l_s)$, where c is the sound speed in the medium. The time decay of $g_1^t(n)$ is a mean to estimate the scattering mean free path l_s, and the total scattering cross section of the scatterer for a diluted medium since $\sigma_T = V/l_s$.

It is shown here that the normalized cross-correlation function $g_1^t(n) = [I_n(t)]/[A(t)]$ is a function of both the total scattering cross section σ_T and the displacement $\delta r(n)$ of the scatterer. Then, we demonstrate that the variance $\Sigma_{In}(t) = \langle (h_k(t) h_{k+n}(t))^2 \rangle - \langle h_k(t) h_{k+n}(t) \rangle^2$ of the cross correlation $h_k(t) h_{k+n}(t)$ can be written as a function of $g_1^t(n)$ and the total scattering cross section σ_T, and used to estimate the average displacement of the scatterer.

1. Normalized cross-correlation function

The expression of the normalized cross-correlation function with the motion of the scatterer was presented by de Rosny *et al.* (2003). The acoustic field $h_k(t)$ can be described as the infinite summation of the contributions $h_k^m(t)$, corresponding to the field scattered m times. In a dilute medium, the contributions $h_k^m(t)$ are uncorrelated between each other, since the scattering events are independent,

$$h_k(t) = \sum_{m=0}^{\infty} h_k^m(t).$$

The total intensity after m scattering events is proportional to $\langle h_k^m(t)^2 \rangle$. Between t and $t+dt$, the total intensity in the cavity will decrease by $(c/l_s)\langle h_k^m(t)^2 \rangle dt$ due to the scattering from the scatterer after m scattering events, and also by $(c/l_a) \times \langle h_k^m(t)^2 \rangle dt$ due to the absorption from the cavity and the scatterer. l_a is the absorption mean free path due to the attenuation in the cavity and the absorption from the scatterer. At the same time, after the first scattering event has occurred $m > 0$, the total intensity increases by $(c/l_s)\langle h_k^{m-1}(t)^2 \rangle dt$ corresponding to the intensity from the $m-1$ preceding scattering events. From these considerations, the following Kolmogoroff system of equations can be written:

$$\frac{d\langle h_k^0(t)^2 \rangle}{dt} = -\left(\frac{c}{l_s} + \frac{c}{l_a} \right) \langle h_k^0(t)^2 \rangle \tag{1}$$

and for $m > 0$

$$\frac{d\langle h_k^m(t)^2 \rangle}{dt} = \frac{c}{l_s} (\langle h_k^{m-1}(t)^2 \rangle - \langle h_k^m(t)^2 \rangle) - \frac{c}{l_a} \langle h_k^m(t)^2 \rangle. \tag{2}$$

The solution for this system is a Markoff–Poisson process

$$\langle h_k^m(t)^2 \rangle = \langle h_k^0(t)^2 \rangle \exp\left(-\frac{tc}{l_s} \right) \frac{(tc/l_s)^m}{m!} \exp\left(-\frac{tc}{l_a} \right). \tag{3}$$

From the independence of the scattering events, $\langle h_k^m(t) h_k^{m'}(t) \rangle = 0$ for $m \neq m'$, the coherent intensity becomes

$$I_n(t) = \langle h_k(t) h_{k+n}(t) \rangle = \sum_{m=0}^{\infty} \langle h_k^m(t) h_{k+n}^m(t) \rangle. \tag{4}$$

The normalized cross-correlation function of the mth scattering event is

$$g_1^{(m)}(n) = \frac{\langle h_k^m(t) h_{k+n}^m(t) \rangle}{\langle h_k^m(t)^2 \rangle}; \tag{5}$$

therefore,

$$\langle h_k(t) h_{k+n}(t) \rangle = \sum_{m=0}^{\infty} \langle h_k^m(t) h_{k+n}^m(t) \rangle = \sum_{m=0}^{\infty} \langle h_k^m(t)^2 \rangle g_1^{(m)}(n), \tag{6}$$

and with Eq. (3)

$$\langle h_k(t) h_{k+n}(t) \rangle = \langle h_k^0(t)^2 \rangle \exp\left(-\frac{tc}{l_s} - \frac{tc}{l_a} \right) \times \left(1 + \sum_{m=1}^{\infty} \frac{(tc/l_s)^m}{m!} g_1^{(m)}(n) \right), \tag{7}$$

with $\langle h_k(t)^2 \rangle = \langle h_k^0(t)^2 \rangle \exp(-tc/l_a)$,

$$g_1^t(n) = \exp\left(-\frac{tc}{l_s} \right) \left(1 + \sum_{m=1}^{\infty} \frac{(tc/l_s)^m}{m!} g_1^{(m)}(n) \right). \tag{8}$$

The normalized cross-correlation $g_1^{(m)}(n)$ is equal to the integral over the possible motion y of the normalized spatial

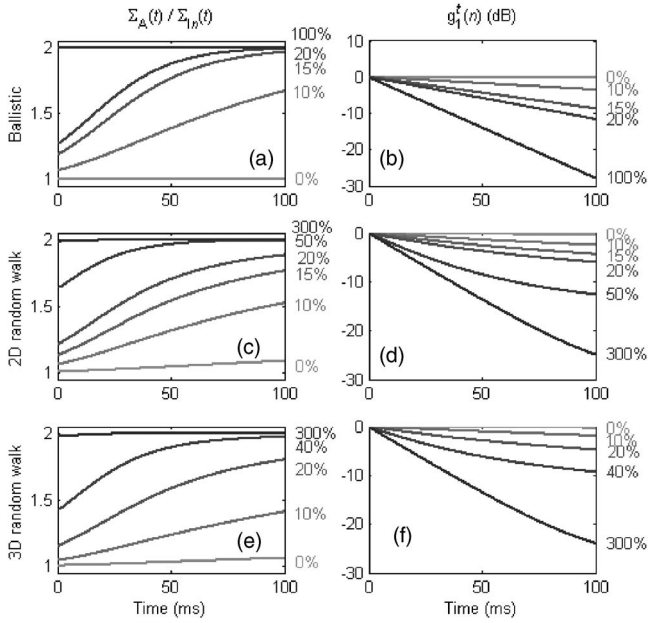

FIG. 1. Theoretical predictions for the ratio $\Sigma_A(t)/\Sigma_{In}(t)$ and $g_1^t(n)$ in the case of a 23-mm copper sphere in 16 liters of water and various displacement amplitudes. (a) and (b): Case of ballistic motion. (c) and (d): Case of 2D random walk. (e) and (f): Case of 3D random walk. The displacement of the scatterer relative to wavelength $\delta x/\lambda$ is comprised between 0% and 300%, from light to dark.

cross-correlation function of the wave field $S_c(y)$ multiplied by the probability for the scatterer to move a distance y after n steps,

$$g_1^{(m)}(n) = \int_0^\infty S_c(y)^m P_n(y) dy. \tag{9}$$

For ballistic motion $\delta r(n) = n\delta x$, and the normalized spatial cross-correlation function of the wave field is $S_c(y) = [\sin(2\pi y/\lambda)/(2\pi y/\lambda)]^2$ (Cook *et al.*, 1955), and the probability $P_n(y)$ is the Dirac function $\delta(y - \delta r(n))$ (de Rosny *et al.*, 2003). In this case, the normalized cross correlation is given by

$$g_1^{(m)}(n) = \exp\left(-\frac{m(2\pi n\delta x/\lambda)^2}{3}\right). \tag{10}$$

Finally, for ballistic motion, the normalized cross-correlation function $g_1^t(n)$ becomes

$$g_1^t(n) = \exp\left(-\frac{tc}{l_s}\left(1 - \exp\left(-\frac{1}{3}\left(2\pi\frac{n\delta x}{\lambda}\right)^2\right)\right)\right). \tag{11}$$

It can be rewritten as a decreasing exponential: $g_1^t(n) = \exp(-\alpha(n)t)$, where the exponential decay with time of $g_1^t(n)$ for ballistic motion [Fig. 1(b)] is given by

$$\alpha(n) = \frac{c\sigma_T}{V}\left(1 - \exp\left(-\frac{1}{3}\left(2\pi\frac{n\delta x}{\lambda}\right)^2\right)\right). \tag{12}$$

In the case of a 2D or 3D random walk with steps δx, the normalized cross-correlation $g_1^{(m)}(n)$ becomes (de Rosny *et al.*, 2003)

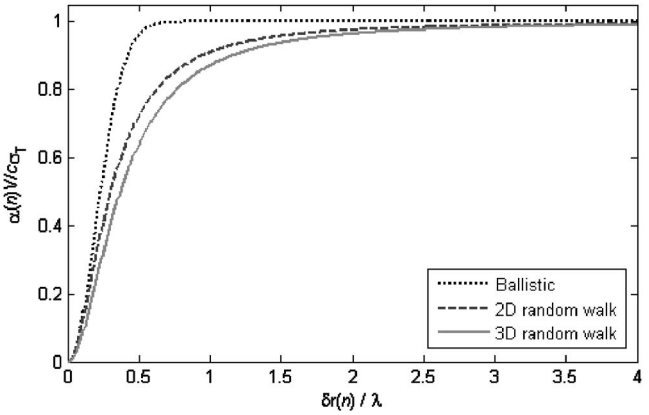

FIG. 2. Theoretical predictions of $\alpha(n)V/c$ normalized to the absolute value σ_T versus displacement of the scatterer $\delta r(n)$ relative to the wavelength λ. Case of ballistic motion (dark dashed) from Eq. (11), 2D random walk (light dashed) from Eq. (16), and 3D random walk (light solid) from Eq. (17).

$$g_1^{(m)}(n) = \frac{1}{1 + \frac{1}{3}m\left(2\pi\frac{\sqrt{n}\delta x}{\lambda}\right)^2} \tag{13}$$

and

$$g_1^{(m)}(n) = \frac{1}{1 + \frac{2}{9}m\left(2\pi\frac{\sqrt{n}\delta x}{\lambda}\right)^2}, \tag{14}$$

respectively. In these cases, no analytical expression can be derived for $g_1^t(n)$. Nevertheless, numerical estimates can be obtained from Eq. (8) [Figs. 1(d) and 1(f)]. The decay with time of $g_1^t(n)$ is not simply exponential anymore. However, for short propagation times, the slope of the semilogarithmic curve is fairly linear. A first-order approximation with tc/l_s yields the exponential decay $\alpha(n)$. Indeed,

$$g_1^t(n) \approx 1 - \frac{tc}{l_s}(1 - g_1^{(1)}(n)) \approx 1 - \alpha(n)t. \tag{15}$$

For a 2D or 3D random walk, $\alpha(n)$ becomes

$$\alpha(n) = \frac{c\sigma_T}{V}\left(1 - \left[1 + \frac{1}{3}(2\pi\sqrt{n}\delta x/\lambda)^2\right]^{-1}\right), \tag{16}$$

and

$$\alpha(n) = \frac{c\sigma_T}{V}\left(1 - \left[1 + \frac{2}{9}(2\pi\sqrt{n}\delta x/\lambda)^2\right]^{-1}\right), \tag{17}$$

respectively. Therefore, measuring the slope at the origin with respect to n is a very convenient and simple way to characterize the motion of the scatterer. For each of the three types of motion, the theoretical predictions for the measurement $\alpha(n)V/c$ are shown in Fig. 2. $\alpha(n)V/c$ tends asymptotically to the absolute σ_T, as the average displacement between acquisitions increases. Hence, the estimate of the total cross section using $\alpha(n)V/c$ is within 4% of the expected value σ_T when the displacement of the scatterer is greater than 0.5, 2, or 3 times the wavelength respectively for ballistic motion, a 2D random walk, or a 3D random walk (Table I).

TABLE I. Percentage of the measurement $\alpha V/c\sigma_T$ for various threshold values of the scatterer displacement δr relative to the wavelength λ. Case of ballistic motion and 2D or 3D random walks.

Motion type	Ballistic	Random walk 2D	Random walk 3D
$\delta r/\lambda$	0.5	2	3
$\alpha V/c\sigma_T$	96.5%	96.7%	97.7%

2. Ratio of the variances

It is of interest to study $\Sigma_{In}(t)$, the variance of the cross correlation $h_k(t)h_{k+n}(t)$. Indeed, we demonstrate that the ratio of the variances $\Sigma_{I0}(t)/\Sigma_{In}(t)$ is mainly sensitive to the scatterer displacement, and not to the total scattering cross section. The variance estimator $\Sigma_{In}(t)$ is given by

$$\Sigma_{In}(t) = \frac{1}{N-n}\sum_{k=1}^{N-n} h_k(t)^2 h_{k+n}(t)^2 - \left(\frac{1}{N-n}\sum_{k=1}^{N-n} h_k(t)h_{k+n}(t)\right)^2. \quad (18)$$

Assuming the $h_k(t)$ are jointly Gaussian variables, and introducing the variance of the autocorrelation $\Sigma_A(t)$ which is equal to $\Sigma_{I0}(t)$, the ratio of the variances is (see the Appendix)

$$\frac{\Sigma_A(t)}{\Sigma_{In}(t)} = 2\frac{1-\exp\left(-2\frac{tc}{l_s}\right)}{1+g_1^t(n)^2-2\exp\left(-2\frac{tc}{l_s}\right)}. \quad (19)$$

For ballistic motion, $g_1^t(n)$ with Eq. (11) gives the following analytical expression for the ratio of the variances:

$$\frac{\Sigma_A(t)}{\Sigma_{In}(t)} = 2\frac{1-\exp\left(-2\frac{tc}{l_s}\right)}{1-\exp\left(-2\frac{tc}{l_s}\right)\left[2-\exp\left(2\frac{tc}{l_s}\exp\left(-\frac{1}{3}\left(2\pi\frac{n\delta x}{\lambda}\right)^2\right)\right)\right]}, \quad (20)$$

as shown in Fig. 1(a).

For 2D or 3D random walks, the analytical formulas for the ratio $\Sigma_A(t)/\Sigma_{In}(t)$ cannot be obtained directly. But, $\Sigma_A(t)/\Sigma_{In}(t)$ can be evaluated numerically, as shown in Figs. 1(c) and 1(e) using Eqs. (13) and (14), respectively.

When the displacement of the scatterer is small, $g_1^t(n)=1$, and $\Sigma_A(t)/\Sigma_{In}(t)$ is slightly larger than 1. When the positions of the scatterer are uncorrelated, $g_1^t(n)=\exp(-tc/l_s)$, and the ratio $\Sigma_A(t)/\Sigma_{In}(t)$ reaches 2.

Since $g_1^t(n)$ depends mainly on the total scattering cross section, its ability to detect a weak scatterer will depend on the total scattering cross section if the displacement of the scatterer is large relative to the wavelength. On the other end, $\Sigma_A(t)/\Sigma_{In}(t)$ mainly depends on the displacement of the scatterer and not on the total scattering cross section. Therefore, this ratio is much more sensitive to a weak scatterer for large displacements. For instance, with either a 23-mm-diameter

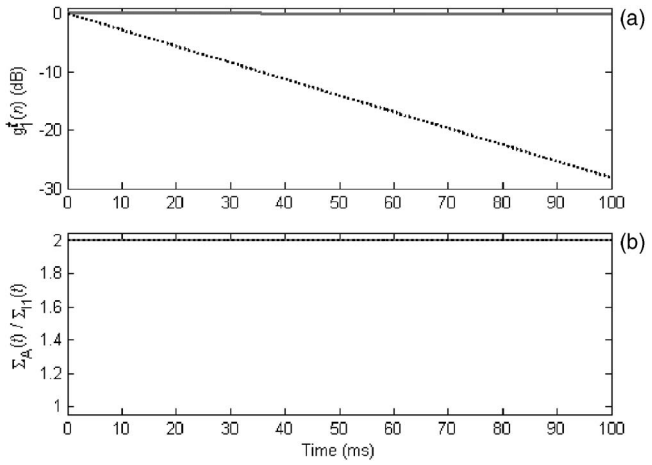

FIG. 3. Theoretical predictions for (a) $g_1^t(n=1)$ and (b) $\Sigma_A(t)/\Sigma_{In}(t)$ for a 23-mm-diameter copper sphere (σ_T=766 mm^2, dark dashed) and a 2-mm-diameter copper sphere (σ_T=5.78 mm^2, light solid) in 16 liters of water. Case of ballistic motion with a displacement of the scatterer relative to wavelength $\delta x/\lambda=3$.

(σ_T=766 mm^2) or a 2-mm-diameter copper sphere (σ_T =5.78 mm^2) in 16 liters of water, following ballistic motion with steps equal to 3 wavelengths, the theoretical predictions for the ratio $\Sigma_A(t)/\Sigma_{In}(t)$ are equal to 2, independently of the total scattering cross section, whereas the decay of $g_1^t(n)$ is too small to be estimated for the small sphere (Fig. 3). Hence, $\Sigma_A(t)/\Sigma_{In}(t)$ is a good metric to detect the motion of a weak scatterer. From a practical point of view, the use of either $g_1^t(n)$ or $\Sigma_A(t)/\Sigma_{In}(t)$ presents different advantages. $\Sigma_A(t)/\Sigma_{In}(t)$ is more sensitive to noise since it is defined from the fourth-order moments. The signal-to-noise ratio is the dominant parameter for practical use of the ratio $\Sigma_A(t)/\Sigma_{In}(t)$. In any case, a sufficiently large signal-to-noise ratio must also be obtained in order to estimate σ_T accurately using $g_1^t(n)$. Therefore, the condition on the signal-to-noise ratio must be verified for both $g_1^t(n)$ and $\Sigma_A(t)/\Sigma_{In}(t)$.

B. Displacement estimation

As shown by Eq. (8), the normalized cross-correlation function $g_1^t(n)$ depends on both the scattering mean free path l_s and the ratio between the displacement of the scatterer δx and the acoustic wavelength λ. If $\delta x/\lambda \gg 1$, the dependence of $g_1^t(n)$ on displacement of the scatterer is negligible. Therefore, when the displacement of the scatterer is large compared to the wavelength, the successive positions are uncorrelated, and the exponential decay of $g_1^t(n)$ leads to the total scattering cross section $\sigma_T = \alpha(n)V/c$ [see Eqs. (12), (16), and (17); Fig. 2]. For smaller displacements of the scatterer, $\delta x/\lambda$ lower than 1, the estimate of the exponential decay $g_1^t(n)$ is a function of n and $\delta x/\lambda$.

As discussed in part Sec. II A, the displacement of the scatterer can be estimated from the measurements of $\alpha(n)$. After n steps of amplitude δx, the actual displacement to consider for $g_1^t(n)$ is $n\delta x$ for ballistic motion, and $2\sqrt{n}\delta x$ or $\sqrt{6n}\delta x$ for 2D or 3D random walks, respectively. A minimization function $D(\delta x)$ can be defined in order to estimate the displacement from these measurements,

$$D(\delta x) = \frac{V}{c\sigma_T} \sum_{n=1}^{n_{\max}} |\bar{\alpha}(n) - \alpha(n, \delta x)|, \tag{21}$$

where $\bar{\alpha}(n)$ is the value measured from the data.

This generalization of the DRAWS method in regard to the fourth-order moments and the estimate of the displacement of the scatterer is tested and confirmed here using experiments for which the displacements of the scatterer are controlled. First, a standard metal sphere is moved by stepping motors. Then, a human walks with controlled steps in a reverberant room. In the case of a group of scatterers, in the limit of a large number of scatterers compared to the scattering order m, $g_1^{(m)}(n)$ is equal to $(\int_0^\infty S_c(y)P_n(y)dy)^m$ (de Rosny *et al.*, 2003).

III. RESULTS

A. Simulations

The simulation was performed using a second-order finite element time-domain scheme for a two-dimensional cavity, similar to the one presented in de Rosny and Roux (2001). There was no absorption in the cavity, therefore $l_a = \infty$. The cavity was a 300- by 300-pixel square, with a spatial resolution of 8 pixels per wavelength (0.125λ per pixel), and Dirichlet boundaries conditions. The sound speed was $c = 1000$ m/s. One emitter transmitted a 50% bandwidth pulse with center frequency $f_c = 1$ kHz. Reverberation time series were recorded using 28 receivers, 2λ apart from each other. The scatterer in the cavity corresponded to 1 pixel, and was defined by the sound-speed contrast $c_{\text{scatterer}}/c$. Since the total scattering cross section of the scatterer σ_T could not be derived theoretically for the simulation due to the heterogeneity of the two-dimensional simulation lattice, σ_T was evaluated using simulations measuring l_s for $K = 0$ to 50 scatterers in the cavity taking random uncorrelated positions. σ_T was obtained from the slope of V/l_s versus number of scatterers since $\sigma_T(K) = V/Kl_s$, with $V = (300 \times 0.125)^2$. For a sound-speed contrast $c_{\text{scatterer}}/c = 0.7$, the total scattering cross section normalized to the wavelength σ_T/λ was 3.122×10^{-2}.

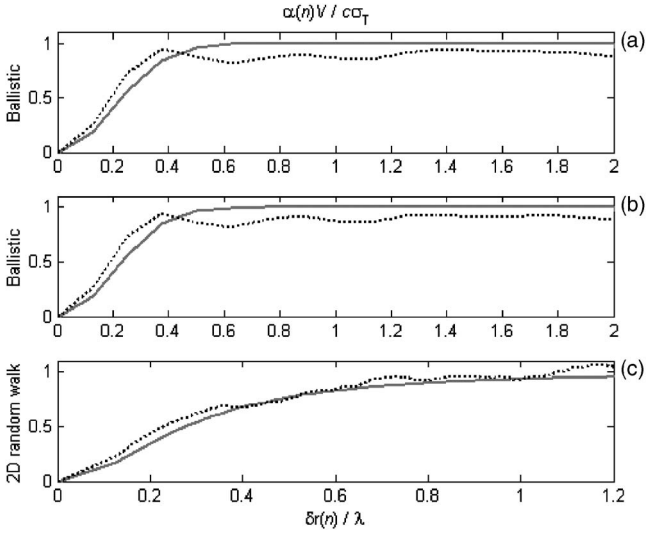

FIG. 4. Measurement of $\alpha(n)V/c$ versus displacement relative to wavelength $\delta r(n)/\lambda$. Case of a 2D simulation for a single scatterer with sound-speed contrast $c_{\text{scatterer}}/c = 0.7$. The measurements (dark dashed) are compared to theoretical predictions (light solid) for (a) and (b) two different ballistic motions, and (c) a 2D random walk. The theoretical predictions are obtained using Eq. (11) for the ballistic motions and Eq. (16) for the random walk.

The same simulation was then used with only one scatterer for two different ballistic displacements and a random walk. In all three cases, the scatterer was moved 1 pixel between consecutive pulses k and $k+1$, corresponding to a displacement $\delta x = \lambda/8$. Ensembles of 200 positions were simulated, but $N = 100$ positions was used for the calculations. Using the pulses k and $k+n$ as consecutive, with n ranging from 1 to 100, the displacement of the scatterer was $\delta r(n) = n\lambda/8$ for the ballistic motion. For the random walk, the average displacement of the scatterer was estimated using the actual positions of the scatterer during the simulation.

The theoretical predictions and the measurements of $\alpha(n)$ versus relative displacement of the scatterer for the two ballistic motions, and the 2D random walk are in good agreement (Fig. 4).

B. Controlled experiments

1. Sphere moved by stepping motors

A first set of experiments was obtained using a 23-mm-diameter copper sphere in a 20-liter stainless-steel bucket filled with approximately 16 liters of fresh water. The transmitted signal was a 15-ms-long chirp between 200 and 800 kHz ($f_c = 500$ kHz, $\lambda/2 = 1.4$ mm), and the transient fields were recorded over 50 ms using an 8-bit resolution oscilloscope for five positions of the receiver. The total scattering cross section was estimated for three narrow frequency bands centered at 300, 500, and 700 kHz with a 10-kHz bandwidth, after filtering the data in the corresponding narrow bands. The sphere was moved using stepping motors. The displacement of the sphere between two consecutive transient fields was $\delta x = 0.1$ mm for a total of 200 positions

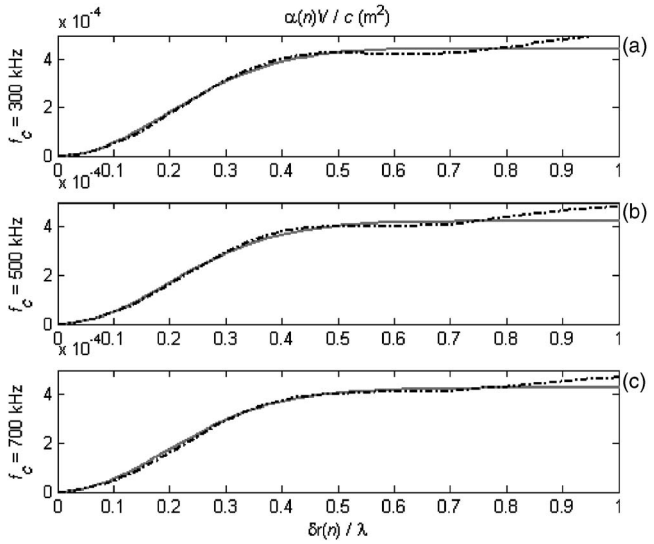

FIG. 5. Estimate of $\alpha(n)V/c$ versus displacement relative to wavelength $\delta r(n)/\lambda$ for a 23-mm-diameter copper sphere following ballistic motion in 16 liters of water. The measurements (dark dashed) are obtained for 10-kHz frequency bands centered at (a) 300; (b) 500; and (c) 700 kHz. Theoretical predictions (light solid) are obtained using Eq. (11).

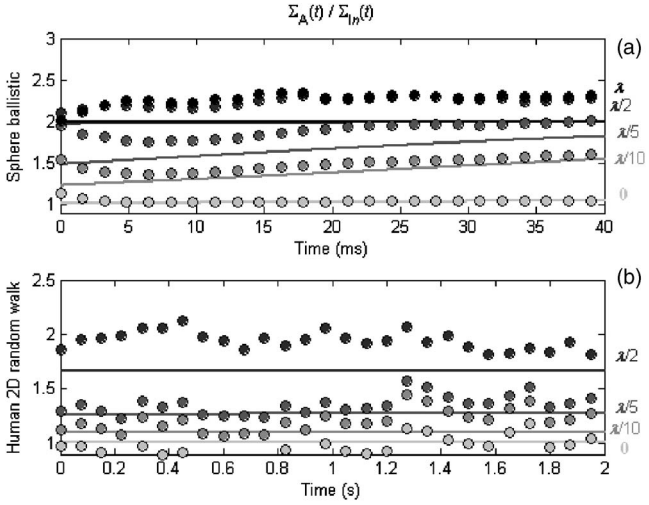

FIG. 6. Ratio of the variances $\Sigma_A(t)/\Sigma_{In}(t)$, experimental results for (a) a 23-mm-diameter copper sphere following a ballistic motion in 16 liters of water at 700 kHz; (b) a human in a squash court for a 2D random walk with 3-cm steps. The points correspond to the experimental measurements, and the straight lines to the theoretical predictions from Eq. (20) for the ballistic motion, and Eqs. (19) and (13) for random walk. The displacement of the scatterer relative to wavelength $\delta x/\lambda$ is 0; 1/10; 1/5; 1/2; and 1, from light to dark.

$(\delta x < \lambda/20)$. Practically, the sphere was moved constantly at a very low speed (0.02 mm/s), and its position was measured continuously with the stepping motor controller. Once the desired position was reached, the emission/acquisition system was triggered, and the measured position of the sphere was compared to the desired one.

The results are in good agreement with the theory for each of the frequency bands centered at 300, 500, and 700 kHz (Fig. 5). For displacement greater than half the wavelength, the measured total scattering cross section corresponds to the expected value. For $\delta r/\lambda > 0.9$ (approximately), the measurements appear to be higher than the expected value. In order to achieve such displacements of the sphere, the time intervals between shots had to be increased. As the time intervals increase, parameters of the medium such as the temperature are more likely to fluctuate. These fluctuations lead to sound-speed fluctuations, and a positive bias in the measurements explaining the higher values for large displacements of the scatterer.

The experimental results for the ratio of the variances $\Sigma_A(t)/\Sigma_{In}(t)$ with the 23-mm copper sphere following ballistic motion at 700 kHz shows a good agreement with theory [Fig. 6(a)]. As the time interval between the time series was increased for the large displacements of the sphere, some discrepancies appeared between the theoretical predictions and the experimental results.

2. Human walking in a reverberant room

A second set of experiments was realized with a human walking in a squash court using the experimental setup presented in Conti *et al.* (2004). Two-second chirps were transmitted between 100 and 500 Hz (f_c=300 Hz, $\lambda/2$=57.5 cm), and ensembles of 100 transient fields were recorded over 5 s using four receivers. During the experiment, a human walked in the room either along a straight line, or following a random walk. In both cases, the human moved between pulses by small steps of δx=3 cm ($\delta x < \lambda/20$), with a 0.5-cm precision (approximately).

For both ballistic motion and 2D random walk, the experimental results with the human walking in the squash court are in good agreement with theory (Fig. 7). For the 2D random walk, the number of transient fields recorded did not provide a larger range for the displacement of the scatterer than the one presented. But, even over this limited range, the measurements and the theory are in good agreement, and sufficient to estimate the average displacement of the human.

For the ratio of the variances $\Sigma_A(t)/\Sigma_{In}(t)$ with the hu-

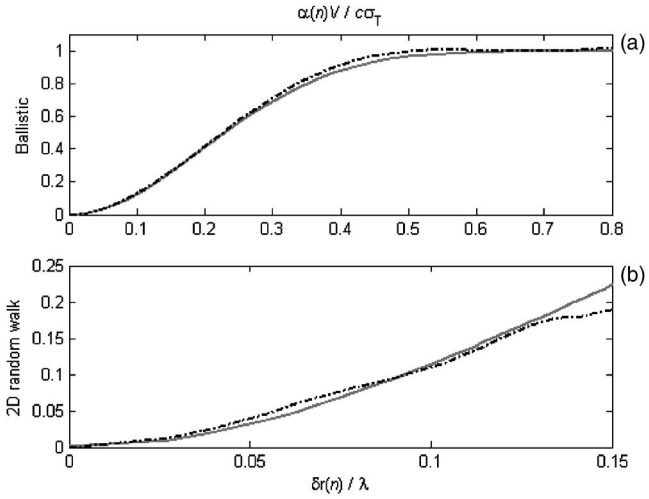

FIG. 7. Normalized measurement of $\alpha(n)V/c\sigma_T$ versus displacement relative to wavelength $\delta r(n)/\lambda$ for a human in a squash court with 3-cm steps. (a) Case of ballistic motion. (b) Case of 2D random walk. The measurements (dark dashed) are obtained between 100 and 500 Hz. Theoretical predictions (light solid) are obtained using Eq. (11) for the ballistic motion, and Eq. (16) for the 2D random walk.

TABLE II. Estimated and expected displacement between shots obtained using the minimization of the function $D(\delta x)$.

Experiment	Estimated displacement	Expected displacement
Copper sphere 300 kHz	0.102 mm	0.1 mm
Copper sphere 500 kHz	0.100 mm	0.1 mm
Copper sphere 700 kHz	0.098 mm	0.1 mm
Human ballistic motion	3.26 cm	3 cm
Human 2D random walk	3.14 cm	3 cm

man following a 2D random walk [Fig. 6(b)], the results are similar to the ones obtained for the 23-mm-diameter copper sphere.

3. Estimating the displacement of the scatterer

Using the function $D(\delta x)$ from Eq. (21), the displacement of the 23-mm copper sphere and the human can be estimated precisely from the acoustical measurements (Table II). With the sphere, $D(\delta x)$ reaches a minimum within a few percent of the actual displacement used during the experiments, independent of the frequency (Fig. 8). Similar results are achieved for the experiments in the squash court with the human (Fig. 9). For the ballistic motion, the estimated displacement is less than 10% higher than the expected value, but the precision on the positions of the human was greater than 10% of the actual displacement (Table II). For the 2D random walk, the estimated displacement corresponds to the expected one within 5%.

IV. CONCLUSION

Using both simulations and experiments in different environments, the dependence with motion of the normalized cross-correlation function $g_1^t(n)$ in a reverberant medium has been demonstrated. These results are obtained for a scatterer following either ballistic motion or random walk. The correlation of the scatterer positions between time series can be evaluated using the ratio of the variances $\Sigma_A(t)/\Sigma_{In}(t)$.

Precise estimates of the displacement are obtained with a metal sphere for a controlled ballistic motion, and with a human for both ballistic motion and 2D random walk. The generalized DRAWS method could be used to monitor the activity of fish in an aquaculture facility remotely.

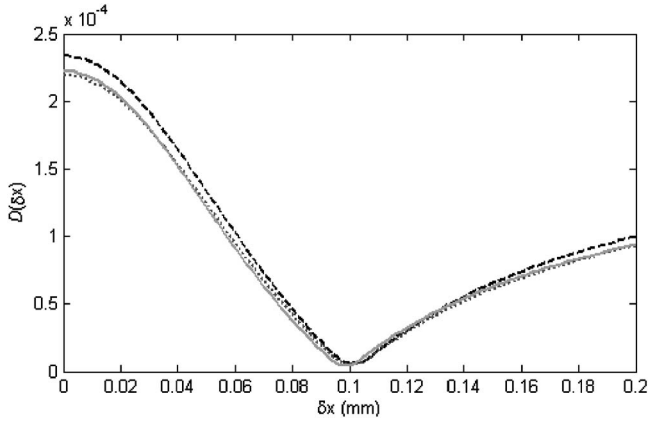

FIG. 8. Function $D(\delta x)$ to estimate the average displacement δx of the 23-mm copper sphere following ballistic motion in 16 liters of water. The results are obtained for three frequency bands centered at 300 (dark dashed), 500 (light dashed), and 700 (light solid) kHz, with a 10-kHz bandwidth.

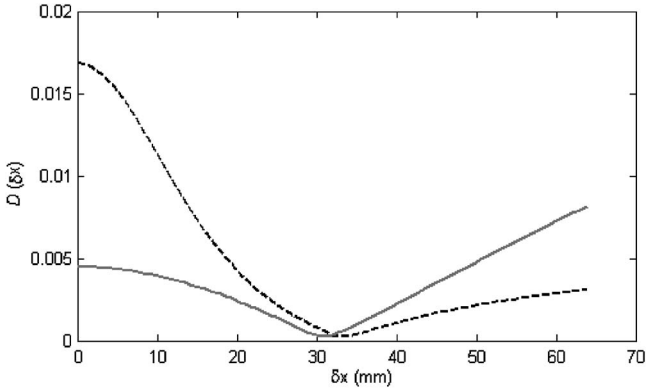

FIG. 9. Function $D(\delta x)$ to estimate the average displacement δx for the human walking in a squash court for ballistic motion (dark dashed), and 2D random walk (light solid).

APPENDIX: THEORETICAL DERIVATION OF THE VARIANCE ESTIMATOR

The variance estimator $\Sigma_{In}(t)$ of the cross correlation $h_k(t)h_{k+n}(t)$ is given by

$$\Sigma_{In}(t) = \frac{1}{N-n}\sum_{k=1}^{N-n} h_k(t)^2 h_{k+n}(t)^2 - \left(\frac{1}{N-n}\sum_{k=1}^{N-n} h_k(t)h_{k+n}(t)\right)^2. \quad \text{(A1)}$$

It can be written as

$$\Sigma_{In}(t) = \langle h_k(t)^2 h_{k+n}(t)^2\rangle - \frac{1}{(N-n)^2}\sum_{k,l=1}^{N-n} h_k(t)h_{k+n}(t)h_l(t)h_{l+n}(t) = \langle h_k(t)^2 h_{k+n}(t)^2\rangle - \langle h_k(t)h_{k+n}(t)h_l(t)h_{l+n}(t)\rangle. \quad \text{(A2)}$$

The moment theorem can be applied to the Gaussian random variables $h_k(t)$, $h_{k+n}(t)$, $h_l(t)$, and $h_{l+n}(t)$, and

$$\langle h_k(t)h_{k+n}(t)h_l(t)h_{l+n}(t)\rangle = \langle h_k(t)h_{k+n}(t)\rangle\langle h_l(t)h_{l+n}(t)\rangle + \langle h_k(t)h_l(t)\rangle\langle h_{k+n}(t)h_{l+n}(t)\rangle + \langle h_k(t)h_{l+n}(t)\rangle\langle h_{k+n}(t)h_l(t)\rangle. \quad \text{(A3)}$$

Each term of this sum can be expressed using the normalized cross-correlation function $g_1^t(n)$ as follows:

$$\langle h_k(t)h_{k+n}(t)\rangle\langle h_l(t)h_{l+n}(t)\rangle = \langle h_k(t)^2\rangle^2 g_1^t(n)^2, \quad \text{(A4)}$$

$$\langle h_k(t)h_l(t)\rangle\langle h_{k+n}(t)h_{l+n}(t)\rangle = \langle h_k(t)^2\rangle^2 g_1^t(\infty)^2, \quad \text{(A5)}$$

$$\langle h_k(t)h_{l+n}(t)\rangle\langle h_l(t)h_{k+n}(t)\rangle = \langle h_k(t)^2\rangle^2 g_1^t(\infty)^2. \quad \text{(A6)}$$

With $k=l$ in Eq. (24)

$$\langle h_k(t)^2 h_{k+n}(t)^2\rangle = \langle h_k(t)^2\rangle^2 + 2\langle h_k(t)h_{k+n}(t)\rangle^2$$
$$= \langle h_k(t)^2\rangle^2(1 + 2g_1^t(n)^2). \quad \text{(A7)}$$

The variance estimator $\Sigma_{In}(t)$ can be written as

$$\Sigma_{In}(t) = \langle h_k(t)^2\rangle^2(1 + g_1^t(n)^2 - 2g_1^t(\infty)^2). \quad \text{(A8)}$$

Since $g_1^t(\infty)=\exp(-tc/l_s)$ and $g_1^t(0)=1$ from Eq. (8), the variance estimator $\Sigma_{In}(t)$ becomes

$$\Sigma_{In}(t) = \langle h_k(t)^2\rangle^2\left(1 + g_1^t(n)^2 - 2\exp\left(-2\frac{tc}{l_s}\right)\right). \quad \text{(A9)}$$

Finally, introducing $\Sigma_A(t)=\Sigma_{I0}(t)$, the variance of the autocorrelation $h_k(t)^2$, the ratio of the variances is

$$\frac{\Sigma_A(t)}{\Sigma_{In}(t)} = 2\frac{1 - \exp\left(-2\frac{tc}{l_s}\right)}{1 + g_1^t(n)^2 - 2\exp\left(-2\frac{tc}{l_s}\right)}. \quad \text{(A10)}$$

Conti, S. G., and Demer, D. A. (**2003**). "Wide-bandwidth acoustical characterization of anchovy and sardine from reverberation measurements in an echoic tank," ICES J. Mar. Sci. **60**(3), 617–624.

Conti, S. G., Demer, D. A., and Brierley, A. S. (**2005**). "Broadbandwidth sound scattering and absorption from krill (*Meganyctiphanes norvegica*), Mysids (*Praunus flexuousus* and *Neomysis integer*) and shrimp (*Crangon crangon*)," ICES J. Mar. Sci. **62**(5), 656–965 .

Conti, S. G., Roux, P., Demer, D. A., and de Rosny, J. (**2004**). "Measurement of the scattering and absorption cross-sections of the human body," Appl. Phys. Lett. **84**, 819–821.

Cook, R., Waterhouse, R., Berendt, R., Edelman, S., and Thompson, M. (**1955**). "Measurements of correlation coefficients in reverberant sound fields," J. Acoust. Soc. Am. **27**, 1072–1077.

Cowan, M. L., Page, J. H., and Weitz, D. A. (**2000**). "Velocity fluctuations in fluidized suspensions probed by ultrasonic correlation spectroscopy," Phys. Rev. Lett. **85**, 453–456.

Cowan, M. L., Jones, I. P., Page, J. H., and Weitz, D. A. (**2002**). "Diffusing acoustic wave spectroscopy," Phys. Rev. E **65**, 066605.

de Rosny, J. (2000). "Milieux réverbérants et réversibilité," Doctoral Thesis, Université Paris VI, p. 156.

de Rosny, J., and Roux, P. (**2001**). "Multiple scattering in a reflecting cavity: Application to fish counting in a tank," J. Acoust. Soc. Am. **109**, 2587–2597.

de Rosny, J., Roux, P., Fink, M., and Page, J. H. (**2003**). "Field fluctuation spectroscopy in a reverberant cavity with moving scatterers," Phys. Rev. Lett. **90**, 094302.

Demer, D. A., and Conti, S. G. (**2003**). "Validation of the stochastic distorted-wave Born approximation model with broad bandwidth total target strength measurements of Antarctic krill," ICES J. Mar. Sci. **60**(3), 625–635.

Demer, D. A., Conti, S. G., de Rosny, J., and Roux, P. (**2003**). "Absolute measurements of total target strength from reverberation in a cavity," J. Acoust. Soc. Am. **113**, 1387–1394.

Ishimaru, A. (**1978**). *Wave Propagation and Scattering in Random Media* Academic, New York, Vols. I and II.

Maret, G., and Wolf, P. E. (**1987**). "Multiple light-scattering from disordered media—the effect of Brownian motion of scatterers," Z. Phys. B: Condens. Matter **65**, 409–431.

Pine, D. J., Weitz, D. A., Chaikin, P. M., and Herbolzheimer, E. (**1988**). "Diffusing wave spectroscopy," Phys. Rev. Lett. **60**, 1134–1137.

Schroeder, M. (**1959**). "Measurement of sound diffusion in reverberation chambers," J. Acoust. Soc. Am. **31**, 1407–1414.

Sheng, P. (**1995**). *Introduction to Wave Scattering, Localization, and Mesoscopic Phenomena* (Academic, New York).